Study of the near-threshold $\omega\phi$ mass enhancement in doubly OZI-suppressed $J/\psi \to \gamma\omega\phi$ decays

M. Ablikim,[1] M. N. Achasov,[6] O. Albayrak,[3] D. J. Ambrose,[39] F. F. An,[1] Q. An,[40] J. Z. Bai,[1] Y. Ban,[26] J. Becker,[2] J. V. Bennett,[16] M. Bertani,[17a] J. M. Bian,[38] E. Boger,[19,*] O. Bondarenko,[20] I. Boyko,[19] R. A. Briere,[3] V. Bytev,[19] X. Cai,[1] O. Cakir,[34a] A. Calcaterra,[17a] G. F. Cao,[1] S. A. Cetin,[34b] J. F. Chang,[1] G. Chelkov,[19,*] G. Chen,[1] H. S. Chen,[1] J. C. Chen,[1] M. L. Chen,[1] S. J. Chen,[24] X. Chen,[26] Y. B. Chen,[1] H. P. Cheng,[14] Y. P. Chu,[1] D. Cronin-Hennessy,[38] H. L. Dai,[1] J. P. Dai,[1] D. Dedovich,[19] Z. Y. Deng,[1] A. Denig,[18] I. Denysenko,[19,†] M. Destefanis,[43a,43c] W. M. Ding,[28] Y. Ding,[22] L. Y. Dong,[1] M. Y. Dong,[1] S. X. Du,[46] J. Fang,[1] S. S. Fang,[1] L. Fava,[43b,43c] C. Q. Feng,[40] R. B. Ferroli,[17a] P. Friedel,[2] C. D. Fu,[1] Y. Gao,[33] C. Geng,[40] K. Goetzen,[7] W. X. Gong,[1] W. Gradl,[18] M. Greco,[43a,43c] M. H. Gu,[1] Y. T. Gu,[9] Y. H. Guan,[36] A. Q. Guo,[25] L. B. Guo,[23] T. Guo,[23] Y. P. Guo,[25] Y. L. Han,[1] F. A. Harris,[37] K. L. He,[1] M. He,[1] Z. Y. He,[25] T. Held,[2] Y. K. Heng,[1] Z. L. Hou,[1] C. Hu,[23] H. M. Hu,[1] J. F. Hu,[35] T. Hu,[1] G. M. Huang,[4] G. S. Huang,[40] J. S. Huang,[12] L. Huang,[1] X. T. Huang,[28] Y. Huang,[24] Y. P. Huang,[1] T. Hussain,[42] C. S. Ji,[40] Q. Ji,[1] Q. P. Ji,[25] X. B. Ji,[1] X. L. Ji,[1] L. L. Jiang,[1] X. S. Jiang,[1] J. B. Jiao,[28] Z. Jiao,[14] D. P. Jin,[1] S. Jin,[1] F. F. Jing,[33] N. Kalantar-Nayestanaki,[20] M. Kavatsyuk,[20] B. Kopf,[2] M. Kornicer,[37] W. Kuehn,[35] W. Lai,[1] J. S. Lange,[35] M. Leyhe,[2] C. H. Li,[1] Cheng Li,[40] Cui Li,[40] D. M. Li,[46] F. Li,[1] G. Li,[1] H. B. Li,[1] J. C. Li,[1] K. Li,[10] Lei Li,[1] Q. J. Li,[1] S. L. Li,[1] W. D. Li,[1] W. G. Li,[1] X. L. Li,[28] X. N. Li,[1] X. Q. Li,[25] X. R. Li,[27] Z. B. Li,[32] H. Liang,[40] Y. F. Liang,[30] Y. T. Liang,[35] G. R. Liao,[33] X. T. Liao,[1] D. Lin,[11] B. J. Liu,[1] C. L. Liu,[3] C. X. Liu,[1] F. H. Liu,[29] Fang Liu,[1] Feng Liu,[4] H. Liu,[1] H. B. Liu,[9] H. H. Liu,[13] H. M. Liu,[1] H. W. Liu,[1] J. P. Liu,[44] K. Liu,[33] K. Y. Liu,[22] Kai Liu,[36] P. L. Liu,[28] Q. Liu,[36] S. B. Liu,[40] X. Liu,[21] Y. B. Liu,[25] Z. A. Liu,[1] Zhiqiang Liu,[1] Zhiqing Liu,[1] H. Loehner,[20] G. R. Lu,[12] H. J. Lu,[14] J. G. Lu,[1] Q. W. Lu,[29] X. R. Lu,[36] Y. P. Lu,[1] C. L. Luo,[23] M. X. Luo,[45] T. Luo,[37] X. L. Luo,[1] M. Lv,[1] C. L. Ma,[36] F. C. Ma,[22] H. L. Ma,[1] Q. M. Ma,[1] S. Ma,[1] T. Ma,[1] X. Y. Ma,[1] F. E. Maas,[11] M. Maggiora,[43a,43c] Q. A. Malik,[42] Y. J. Mao,[26] Z. P. Mao,[1] J. G. Messchendorp,[20] J. Min,[1] T. J. Min,[1] R. E. Mitchell,[16] X. H. Mo,[1] C. Morales Morales,[11] N. Yu. Muchnoi,[6] H. Muramatsu,[39] Y. Nefedov,[19] C. Nicholson,[36] I. B. Nikolaev,[6] Z. Ning,[1] S. L. Olsen,[27] Q. Ouyang,[1] S. Pacetti,[17b] J. W. Park,[27] M. Pelizaeus,[2] H. P. Peng,[40] K. Peters,[7] J. L. Ping,[23] R. G. Ping,[1] R. Poling,[38] E. Prencipe,[18] M. Qi,[24] S. Qian,[1] C. F. Qiao,[36] L. Q. Qin,[28] X. S. Qin,[1] Y. Qin,[26] Z. H. Qin,[1] J. F. Qiu,[1] K. H. Rashid,[42] G. Rong,[1] X. D. Ruan,[9] A. Sarantsev,[19,‡] B. D. Schaefer,[16] M. Shao,[40] C. P. Shen,[37,§] X. Y. Shen,[1] H. Y. Sheng,[1] M. R. Shepherd,[16] X. Y. Song,[1] S. Spataro,[43a,43c] B. Spruck,[35] D. H. Sun,[1] G. X. Sun,[1] J. F. Sun,[12] S. S. Sun,[1] Y. J. Sun,[40] Y. Z. Sun,[1] Z. J. Sun,[1] Z. T. Sun,[40] C. J. Tang,[30] X. Tang,[1] I. Tapan,[34c] E. H. Thorndike,[39] D. Toth,[38] M. Ullrich,[35] G. S. Varner,[37] B. Q. Wang,[26] D. Wang,[26] D. Y. Wang,[26] K. Wang,[1] L. L. Wang,[1] L. S. Wang,[1] M. Wang,[28] P. Wang,[1] P. L. Wang,[1] Q. J. Wang,[1] S. G. Wang,[26] X. F. Wang,[33] X. L. Wang,[40] Y. F. Wang,[1] Z. Wang,[1] Z. G. Wang,[1] Z. Y. Wang,[1] D. H. Wei,[8] J. B. Wei,[26] P. Weidenkaff,[18] Q. G. Wen,[40] S. P. Wen,[1] M. Werner,[35] U. Wiedner,[2] L. H. Wu,[1] N. Wu,[1] S. X. Wu,[40] W. Wu,[25] Z. Wu,[1] L. G. Xia,[33] Z. J. Xiao,[23] Y. G. Xie,[1] Q. L. Xiu,[1] G. F. Xu,[1] G. M. Xu,[26] Q. J. Xu,[10] Q. N. Xu,[36] X. P. Xu,[31] Z. R. Xu,[40] F. Xue,[4] Z. Xue,[1] L. Yan,[40] W. B. Yan,[40] Y. H. Yan,[15] H. X. Yang,[1] Y. Yang,[4] Y. X. Yang,[8] H. Ye,[1] M. Ye,[1] M. H. Ye,[5] B. X. Yu,[1] C. X. Yu,[25] H. W. Yu,[26] J. S. Yu,[21] S. P. Yu,[28] C. Z. Yuan,[1] Y. Yuan,[1] A. A. Zafar,[42] A. Zallo,[17a] Y. Zeng,[15] B. X. Zhang,[1] B. Y. Zhang,[1] C. Zhang,[24] C. C. Zhang,[1] D. H. Zhang,[1] H. H. Zhang,[32] H. Y. Zhang,[1] J. Q. Zhang,[1] J. W. Zhang,[1] J. Y. Zhang,[1] J. Z. Zhang,[1] R. Zhang,[36] S. H. Zhang,[1] X. J. Zhang,[1] X. Y. Zhang,[28] Y. Zhang,[1] Y. H. Zhang,[1] Z. P. Zhang,[40] Z. Y. Zhang,[44] Zhenghao Zhang,[4] G. Zhao,[1] H. S. Zhao,[1] J. W. Zhao,[1] K. X. Zhao,[23] Lei Zhao,[40] Ling Zhao,[1] M. G. Zhao,[25] Q. Zhao,[1] Q. Z. Zhao,[9] S. J. Zhao,[46] T. C. Zhao,[1] Y. B. Zhao,[1] Z. G. Zhao,[40] A. Zhemchugov,[19,*] B. Zheng,[41] J. P. Zheng,[1] Y. H. Zheng,[36] B. Zhong,[23] Z. Zhong,[9] L. Zhou,[1] X. K. Zhou,[36] X. R. Zhou,[40] C. Zhu,[1] K. Zhu,[1] K. J. Zhu,[1] S. H. Zhu,[1] X. L. Zhu,[33] Y. C. Zhu,[40] Y. M. Zhu,[25] Y. S. Zhu,[1] Z. A. Zhu,[1] J. Zhuang,[1] B. S. Zou,[1] and J. H. Zou[1]

(BESIII Collaboration)

[1]*Institute of High Energy Physics, Beijing 100049, People's Republic of China*
[2]*Bochum Ruhr-University, D-44780 Bochum, Germany*
[3]*Carnegie Mellon University, Pittsburgh, Pennsylvania 15213, USA*
[4]*Central China Normal University, Wuhan 430079, People's Republic of China*
[5]*China Center of Advanced Science and Technology, Beijing 100190, People's Republic of China*
[6]*G.I. Budker Institute of Nuclear Physics SB RAS (BINP), Novosibirsk 630090, Russia*
[7]*GSI Helmholtzcentre for Heavy Ion Research GmbH, D-64291 Darmstadt, Germany*
[8]*Guangxi Normal University, Guilin 541004, People's Republic of China*
[9]*GuangXi University, Nanning 530004, People's Republic of China*
[10]*Hangzhou Normal University, Hangzhou 310036, People's Republic of China*
[11]*Helmholtz Institute Mainz, Johann-Joachim-Becher-Weg 45, D-55099 Mainz, Germany*

[12]*Henan Normal University, Xinxiang 453007, People's Republic of China*
[13]*Henan University of Science and Technology, Luoyang 471003, People's Republic of China*
[14]*Huangshan College, Huangshan 245000, People's Republic of China*
[15]*Hunan University, Changsha 410082, People's Republic of China*
[16]*Indiana University, Bloomington, Indiana 47405, USA*
[17a]*INFN Laboratori Nazionali di Frascati, I-00044 Frascati, Italy*
[17b]*INFN and University of Perugia, I-06100 Perugia, Italy*
[18]*Johannes Gutenberg University of Mainz, Johann-Joachim-Becher-Weg 45, D-55099 Mainz, Germany*
[19]*Joint Institute for Nuclear Research, 141980 Dubna, Moscow region, Russia*
[20]*KVI, University of Groningen, NL-9747 AA Groningen, The Netherlands*
[21]*Lanzhou University, Lanzhou 730000, People's Republic of China*
[22]*Liaoning University, Shenyang 110036, People's Republic of China*
[23]*Nanjing Normal University, Nanjing 210023, People's Republic of China*
[24]*Nanjing University, Nanjing 210093, People's Republic of China*
[25]*Nankai University, Tianjin 300071, People's Republic of China*
[26]*Peking University, Beijing 100871, People's Republic of China*
[27]*Seoul National University, Seoul 151-747, Korea*
[28]*Shandong University, Jinan 250100, People's Republic of China*
[29]*Shanxi University, Taiyuan 030006, People's Republic of China*
[30]*Sichuan University, Chengdu 610064, People's Republic of China*
[31]*Soochow University, Suzhou 215006, People's Republic of China*
[32]*Sun Yat-Sen University, Guangzhou 510275, People's Republic of China*
[33]*Tsinghua University, Beijing 100084, People's Republic of China*
[34a]*Ankara University, Dogol Caddesi, 06100 Tandogan, Ankara, Turkey*
[34b]*Dogus University, 34722 Istanbul, Turkey*
[34c]*Uludag University, 16059 Bursa, Turkey*
[35]*Universitaet Giessen, D-35392 Giessen, Germany*
[36]*University of Chinese Academy of Sciences, Beijing 100049, People's Republic of China*
[37]*University of Hawaii, Honolulu, Hawaii 96822, USA*
[38]*University of Minnesota, Minneapolis, Minnesota 55455, USA*
[39]*University of Rochester, Rochester, New York 14627, USA*
[40]*University of Science and Technology of China, Hefei 230026, People's Republic of China*
[41]*University of South China, Hengyang 421001, People's Republic of China*
[42]*University of the Punjab, Lahore 54590, Pakistan*
[43a]*University of Turin, I-10125 Turin, Italy*
[43b]*University of Eastern Piedmont, I-15121 Alessandria, Italy*
[43c]*INFN, I-10125 Turin, Italy*
[44]*Wuhan University, Wuhan 430072, People's Republic of China*
[45]*Zhejiang University, Hangzhou 310027, People's Republic of China*
[46]*Zhengzhou University, Zhengzhou 450001, People's Republic of China*

(Received 24 November 2012; published 22 February 2013)

A 2.25×10^8 J/ψ event sample accumulated with the BESIII detector is used to study the doubly Okubo-Zweig-Iizuka-suppressed decay modes $J/\psi \to \gamma\omega\phi$, $\omega \to \pi^+\pi^-\pi^0$, $\phi \to K^+K^-$. A strong deviation ($> 30\sigma$) from three-body $J/\psi \to \gamma\omega\phi$ phase space is observed near the $\omega\phi$ mass threshold that is consistent with a previous observation reported by the BESII experiment. A partial wave analysis with a tensor covariant amplitude that assumes that the enhancement is due to the presence of a resonance, the $X(1810)$, is performed and confirms that the spin-parity of the $X(1810)$ is 0^{++}. The mass and width of the $X(1810)$ are determined to be $M = 1795 \pm 7(\text{stat})^{+13}_{-5}(\text{syst}) \pm 19(\text{mod})$ MeV/c^2 and $\Gamma = 95 \pm 10(\text{stat})^{+21}_{-34}(\text{syst}) \pm 75(\text{mod})$ MeV/c^2, respectively, and the product branching fraction is measured to be $\mathcal{B}(J/\psi \to \gamma X(1810)) \times \mathcal{B}(X(1810) \to \omega\phi) = (2.00 \pm 0.08(\text{stat})^{+0.45}_{-1.00}(\text{syst}) \pm 1.30(\text{mod})) \times 10^{-4}$. These results are consistent within errors with those of the BESII experiment.

DOI: 10.1103/PhysRevD.87.032008 PACS numbers: 13.40.Hq, 13.25.Gv, 14.40.Be

[*]Also at Moscow Institute of Physics and Technology, Moscow 141700, Russia.
[†]On leave from the Bogolyubov Institute for Theoretical Physics, Kiev 03680, Ukraine.
[‡]Also at PNPI, Gatchina 188300, Russia.
[§]Present address: Nagoya University, Nagoya 464-8601, Japan.

I. INTRODUCTION

An anomalous near-threshold enhancement in the $\omega\phi$ invariant-mass spectrum in the process $J/\psi \to \gamma\omega\phi$ was reported by the BESII experiment [1]. A partial wave analysis (PWA) that used a helicity covariant amplitude that assumed that the enhancement was produced by a resonance, denoted as the $X(1810)$, was performed on the BESII event sample. The analysis indicated that the $X(1810)$ quantum number assignment favored $J^{PC} = 0^{++}$ over $J^{PC} = 0^{-+}$ or 2^{++} with a significance of more than 10σ. The mass and width were determined to be $M = 1812^{+19}_{-26}(\text{stat}) \pm 18(\text{syst})$ MeV/c^2 and $\Gamma = 105 \pm 20(\text{stat}) \pm 28(\text{syst})$ MeV/c^2, respectively, and the product branching fraction $\mathcal{B}(J/\psi \to \gamma X(1810)) \times \mathcal{B}(X(1810) \to \omega\phi) = [2.61 \pm 0.27(\text{stat}) \pm 0.65(\text{syst})] \times 10^{-4}$ was measured. The $J/\psi \to \gamma\omega\phi$ decay mode is a doubly Okubo-Zweig-Iizuka (OZI)-suppressed process with a production rate that is expected to be suppressed relative to $J/\psi \to \gamma\omega\omega$ or $J/\psi \to \gamma\phi\phi$ by at least one order of magnitude [2]. Possible interpretations of the $\omega\phi$ threshold enhancement include a new type of resonance, such as a tetraquark state (with structure $q^2\bar{q}^2$) [3], a hybrid [4], or a glueball state [5] etc., a dynamical effect arising from intermediate meson rescattering [6], a manifestation of the $f_0(1710)$ below threshold [7], or a threshold cusp of an attracting resonance [8]. As of now none of these interpretations has either been established or ruled out by experiment.

A search for the $X(1810)$ was performed by the Belle collaboration in the decay of $B^{\pm} \to K^{\pm}\omega\phi$ [9], but no obvious $X(1810)$ signal was observed. A high statistics data sample collected with the BESIII detector provides a good opportunity to confirm the existence of the $\omega\phi$ threshold enhancement, study its properties and search for other possible related states that decay to $\omega\phi$.

In this paper we present a PWA that uses a tensor covariant amplitude for the $J/\psi \to \gamma\omega\phi$ process, where the ϕ is reconstructed from K^+K^- and the ω from $\pi^+\pi^-\pi^0$. The analysis is based on a sample of $(225.3 \pm 2.8) \times 10^6 J/\psi$ events [10] accumulated with the new Beijing Spectrometer (BESIII) [11] located at the Beijing Electron-Positron Collider (BEPCII) [12], with a center of mass energy of e^+e^- beams $\sqrt{s} = 3.097$ GeV corresponding to J/ψ mass.

II. DETECTOR SETUP AND MONTE CARLO SIMULATION

BEPCII is a double-ring e^+e^- collider designed to provide a peak luminosity of 10^{33} cm^{-2} s^{-1} with beam currents of 0.93 A. The BESIII detector has a geometrical acceptance of 93% of 4π and has four main components: (1) a small-cell, helium-based (40% He, 60% C_3H_8) main drift chamber with 43 layers providing an average single-hit resolution of 135 μm, charged-particle momentum resolution in a 1 T magnetic field of 0.5% at 1 GeV/c, and a dE/dx resolution better than 6%. (2) An electromagnetic calorimeter (EMC) consisting of 6240 CsI(Tl) crystals in a cylindrical structure (barrel) and two end caps. The energy resolution for 1.0 GeV γ-rays is 2.5% (5%) in the barrel (end caps), and the position resolution is 6 mm (9 mm) in the barrel (end caps). (3) A time-of-flight system (TOF) constructed of 5-cm-thick plastic scintillators, with 176 detectors of 2.4 m length in two layers in the barrel and 96 fan-shaped detectors in the end caps. The barrel (end cap) time resolution of 80 ps (110 ps) provides 2σ K/π separation for momenta up to $\sim$1.0 GeV/c. (4) The muon system consists of 1000 m^2 of resistive plate chambers in nine barrels and eight end cap layers and provides 2 cm position resolution.

In this analysis, a GEANT4-based [13] Monte Carlo (MC) simulation software package, boost [14], is used. It provides an event generator, contains the detector geometry description, and simulates the detector response and signal digitization. The production of the J/ψ resonance is simulated by the Monte Carlo event generator KKMC [15,16], while the decays are generated by BesEvtGen [17] for known decay modes with branching ratios set at the Particle Data Group (PDG) [18] world average values, and by the Lund-Charm model [19] for the remaining unknown decays. The analysis is performed in the framework of the BESIII Offline Software System, which takes care of the detector calibration, event reconstruction, and data storage.

III. EVENT SELECTION

Signal $J/\psi \to \gamma\omega\phi$ events with $\phi \to K^+K^-$ and $\omega \to \pi^+\pi^-\pi^0$ final states have the topology $3\gamma K^+K^-\pi^+\pi^-$. The event candidates are required to have four well-reconstructed charged tracks with net charge zero, and at least three photons.

Charged-particle tracks in the polar angle range $|\cos\theta| < 0.93$ are reconstructed from the main drift chamber hits. Only the tracks with points of closest approach to the beam line that are within ± 10 cm of the interaction point in the beam direction, and within 1 cm in the plane perpendicular to the beam are selected. TOF and dE/dx information are combined to form particle identification confidence levels for π, K and p hypotheses. Kaons are identified by requiring the particle identification probability (Prob) to be $\text{Prob}(K) > \text{Prob}(\pi)$ and $\text{Prob}(K) > \text{Prob}(p)$. Two identified Kaons with opposite charges are required.

Photon candidates are reconstructed by clustering signals in EMC crystals. The energy deposited in the nearby TOF counters is included to improve the photon reconstruction efficiency and its energy resolution. The photon candidates are required to be in the barrel region ($|\cos\theta| < 0.8$) of the EMC with at least 25 MeV total energy deposition, or in the end cap regions ($0.86 < |\cos\theta| < 0.92$) with at least 50 MeV total energy deposition, where θ is the polar angle of the shower. The photon candidates are

furthermore required to be isolated from all charged tracks by an angle $>10°$ to suppress showers generated by charged particles. The showers in the region between the barrel and the end caps of the EMC are poorly measured and excluded. Timing information from the EMC is used to suppress electronic noise and energy deposits that are unrelated to the event. Events with at least three good photon candidates are selected.

A four-constraint (4C) energy-momentum conserving kinematic fit is performed to the $3\gamma K^+K^-\pi^+\pi^-$ hypothesis. For events with more than three photon candidates, the candidate combination with the minimum χ^2_{4C} is selected, and it is required that $\chi^2_{4C} < 40$ (the requirement is determined by optimizing $S/\sqrt{S+B}$, where S is the number of MC signal events generated with phase space and $(S+B)$ is the number of signal plus background candidate events in the data). In order to remove background stemming from $J/\psi \to 2\gamma K^+K^-\pi^+\pi^-$ and $J/\psi \to 4\gamma K^+K^-\pi^+\pi^-$, we performed 4C kinematic fits for the hypotheses of $2\gamma K^+K^-\pi^+\pi^-$ and $4\gamma K^+K^-\pi^+\pi^-$ (for the events that have at least four good photon candidates). We require $\chi^2_{4C}(3\gamma K^+K^-\pi^+\pi^-) < \chi^2_{4C}(2\gamma K^+K^-\pi^+\pi^-)$ and $\chi^2_{4C}(3\gamma K^+K^-\pi^+\pi^-) < \chi^2_{4C}(4\gamma K^+K^-\pi^+\pi^-)$, respectively. The π^0 candidates are reconstructed from two of the three selected photons with invariant mass closest to the π^0 mass, and $|M_{\gamma\gamma} - M_{\pi^0}| < 20$ MeV/c^2 is required.

A scatter plot of the $M_{K^+K^-}$ versus $M_{\pi^+\pi^-\pi^0}$ invariant masses for events that survive the above selection criteria is shown in Fig. 1(a). One cluster of events populates the $\phi\phi$ region, which arises from the well-known process $J/\psi \to \gamma\phi\phi$ (one $\phi \to \pi^+\pi^-\pi^0$, the other $\phi \to K^+K^-$), and another cluster of events shows up in the $\omega\phi$ signal region. Since the decays of $J/\psi \to \omega\phi$ and $J/\psi \to \pi^0\omega\phi$ are forbidden by C parity conservation, the observed events in the $\omega\phi$ region are an unambiguous signal for the radiative decay process $J/\psi \to \gamma\omega\phi$. The mass window requirements (I) $|M_{\pi^+\pi^-\pi^0} - M_\omega| < 40$ MeV/c^2 and (II) $|M_{K^+K^-} - M_\phi| < 15$ MeV/c^2 (the requirements are determined by optimizing $S/\sqrt{S+B}$) are defined for the ω and ϕ signal region, respectively, while the requirements of (III) 60 MeV/$c^2 < |M_{\pi^+\pi^-\pi^0} - M_\omega| < 140$ MeV/c^2 and (IV) 1045 MeV/$c^2 < M_{K^+K^-} < 1075$ MeV/c^2 are defined for the ω and ϕ sideband regions, respectively. Figure 1(b) shows the K^+K^- invariant-mass distribution for events in which the $\pi^+\pi^-\pi^0$ invariant-mass lies within the ω signal range (requirement I); here a ϕ signal can clearly be seen. The shaded histogram in Fig. 1(b) shows the corresponding distribution for events within the ω sideband region (requirement III). A small ϕ signal from the $J/\psi \to \gamma\phi\pi^+\pi^-\pi^0$ background is evident. Figure 1(c) shows the $\pi^+\pi^-\pi^0$ invariant-mass distribution for events with K^+K^- invariant-mass within the ϕ signal range (requirement II). As expected, ω and ϕ signals are clearly seen. A small η signal is also observed; this comes from the decay chain $J/\psi \to \gamma\eta K^+K^-(\eta \to \pi^+\pi^-\pi^0)$. The shaded histogram in Fig. 1(c) shows the corresponding distribution for the events within the ϕ sideband region (requirement IV). For events that survive the ω and ϕ requirements on the $\pi^+\pi^-\pi^0$ and K^+K^- invariant mass (requirements I and II), respectively, the $\gamma\pi^+\pi^-\pi^0$ invariant-mass distribution is shown in Fig. 2(a). Here an η' peak is observed; this comes from the decay chain $J/\psi \to \phi\eta'(\phi \to K^+K^-, \eta' \to \gamma\omega, \omega \to \pi^+\pi^-\pi^0)$. To characterize these events, a large MC sample of $J/\psi \to \phi\eta'$ is generated with a flat angular distribution. These have a $K^+K^-\pi^+\pi^-\pi^0$ invariant-mass distribution that is concentrated at masses higher than 2.5 GeV/c^2 and have no impact on the $\omega\phi$ mass-threshold region of interest. A further requirement $M(\gamma\pi^+\pi^-\pi^0) > 1.0$ GeV/c^2 (requirement V) is imposed to remove background from $J/\psi \to \phi\eta'$. Figure 2(b) shows the invariant mass of $K^+K^-\pi^+\pi^-\pi^0$ for events with requirements I, II, and V applied, where a peaking structure near the $\omega\phi$ invariant-mass threshold is observed. The solid histogram in the figure shows the $K^+K^-\pi^+\pi^-\pi^0$ invariant-mass distribution without requirement V. The invariant-mass distribution is very

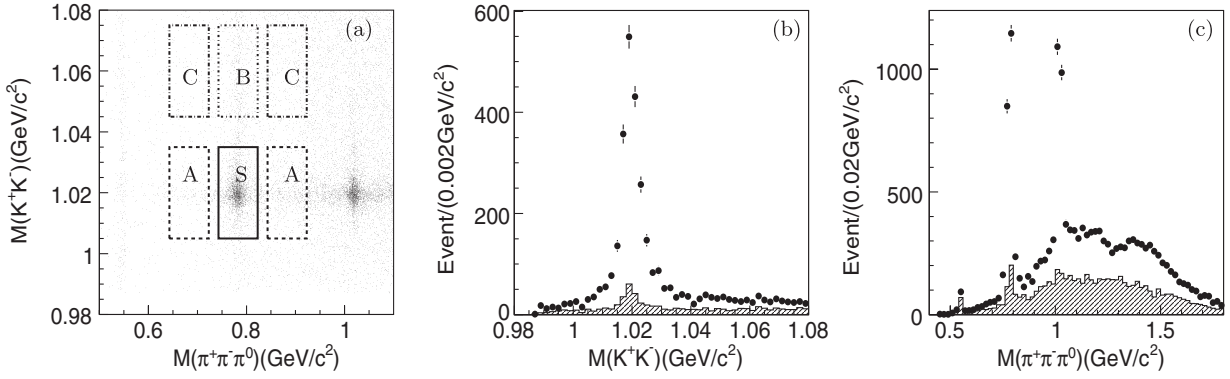

FIG. 1. (a) A scatter plot of $M_{K^+K^-}$ versus $M_{\pi^+\pi^-\pi^0}$. The boxes indicate the signal region labeled as S and sideband regions labeled as A, B, and C (defined in text). (b) The K^+K^- invariant-mass distribution; the shaded histogram shows the events within the ω sideband region. (c) The $\pi^+\pi^-\pi^0$ invariant mass distribution; the shaded histogram shows the events within the ϕ sideband region.

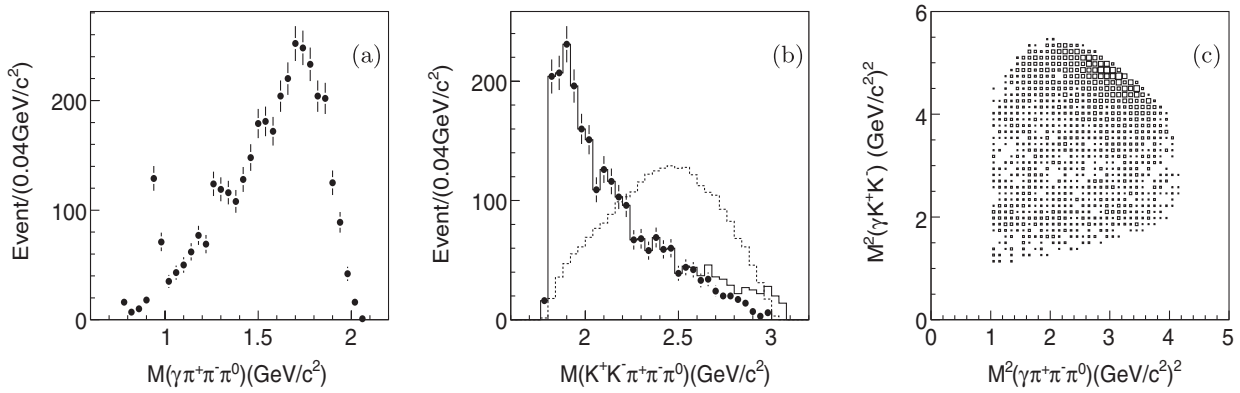

FIG. 2. (a) The $\gamma\pi^+\pi^-\pi^0$ invariant-mass distribution. (b) The $K^+K^-\pi^+\pi^-\pi^0$ invariant-mass distribution; the dashed line is the mass distribution of the phase space MC sample; the solid histogram shows the mass distribution without the $M(\gamma\pi^+\pi^-\pi^0) > 1.0$ GeV/c^2 requirement. (c) A Dalitz plot of $M^2(\gamma\pi^+\pi^-\pi^0)$ *versus* $M^2(\gamma K^+K^-)$.

different from a pure phase-space distribution from MC (dashed histogram, arbitrarily scaled). The threshold structure shows up as a diagonal band along the upper right-hand edge of the Dalitz plot in Fig. 2(c).

The observed $\omega\phi$ mass-threshold enhancement is similar to that observed by the BESII experiment [1]. To ensure that the enhancement is not due to some background process, detailed studies of potential background sources have been performed using both data and MC. Non-ω and non-ϕ backgrounds are studied using ω and ϕ sideband data. Figures 3(a) and 3(b) show the $K^+K^-\pi^+\pi^-\pi^0$ invariant mass for events in the ω sideband region [labeled as Box A in Fig. 1(a)] and the ϕ sideband region [labeled as Box B in Fig. 1(a)]; these are used to determine the non-ω and non-ϕ background contamination in the signal regions. Figure 3(d) shows the same distribution for events in the corner region [labeled as Box C in Fig. 1(a)], for which both the K^+K^- and the $\pi^+\pi^-\pi^0$ invariant masses are in the ϕ and ω sidebands; these are used to estimate the non-ϕ non-ω background. The background contamination in the signal region is estimated to be the sum of the Figs. 3(a) and 3(b) sideband distributions with the Fig. 3(d) distribution subtracted to account for double counting of non-ϕ non-ω background in Figs. 3(a) and 3(b). Phase-space-MC-determined normalization factors are applied that account for differences in the sizes of the selected regions and the difference in the available phase space in the signal and sideband regions. The background contamination in the signal region determined in this way is shown as a solid histogram in Fig. 3(d). The shape of the estimated background is very different from that of data in the signal region, and no evidence of an enhancement near the $\omega\phi$ mass threshold is observed from the non-ω and non-ϕ background events in the data.

An inclusive-decay MC sample of 225 M J/ψ events generated according to the Lund-Charm model [19] and the PDG decay tables is also used to study the potential backgrounds. The dashed histogram in Fig. 3(d) shows the $K^+K^-\pi^+\pi^-\pi^0$ invariant-mass distribution for the selected inclusive J/ψ decay MC events, where no peaking background at the $\omega\phi$ invariant-mass threshold is observed. Exclusive background MC samples of J/ψ decays that have similar final states are generated to further investigate possible background sources. The main backgrounds come from $J/\psi \to \omega K^*K$, $K^* \to K\pi^0$ and $J/\psi \to \omega f_1(1420)$, $f_1(1420) \to K^+K^-\pi^0$ events. For these, the $K^+K^-\pi^+\pi^-\pi^0$ invariant-mass distribution peaks at high masses, and none of these channels produce peaking structures at the $\omega\phi$ mass threshold.

IV. PARTIAL WAVE ANALYSIS

A PWA was performed on the selected $J/\psi \to \gamma\omega\phi$ candidate events to study the properties of the $\omega\phi$ mass-threshold enhancement. In the PWA, we assume the enhancement is due to the presence of a resonance, denoted as X, and the decay processes are described with sequential two-body or three-body decays: $J/\psi \to \gamma X$, $X \to \omega\phi$, $\omega \to \pi^+\pi^-\pi^0$, and $\phi \to K^+K^-$. The amplitudes of the two-body or three-body decays are constructed with a covariant tensor amplitude method [20]. The intermediate structure X is parametrized with the Breit-Wigner propagator

$$BW = 1/(M^2 - s - iM\Gamma), \tag{1}$$

with constant width, where s is the $\omega\phi$ invariant mass-squared, and M and Γ are the resonance mass and width, respectively. The amplitude for the sequential decay process is the product of all decay amplitudes together with the Breit-Wigner propagator. The total differential cross section $d\sigma/d\Phi$ for the process is the square of the linear sum of all possible partial wave amplitudes,

$$\frac{d\sigma}{d\Phi} = \left|\sum A(J^{PC})\right|^2, \tag{2}$$

where $A(J^{PC})$ is the total amplitude for all possible resonances with given J^{PC}.

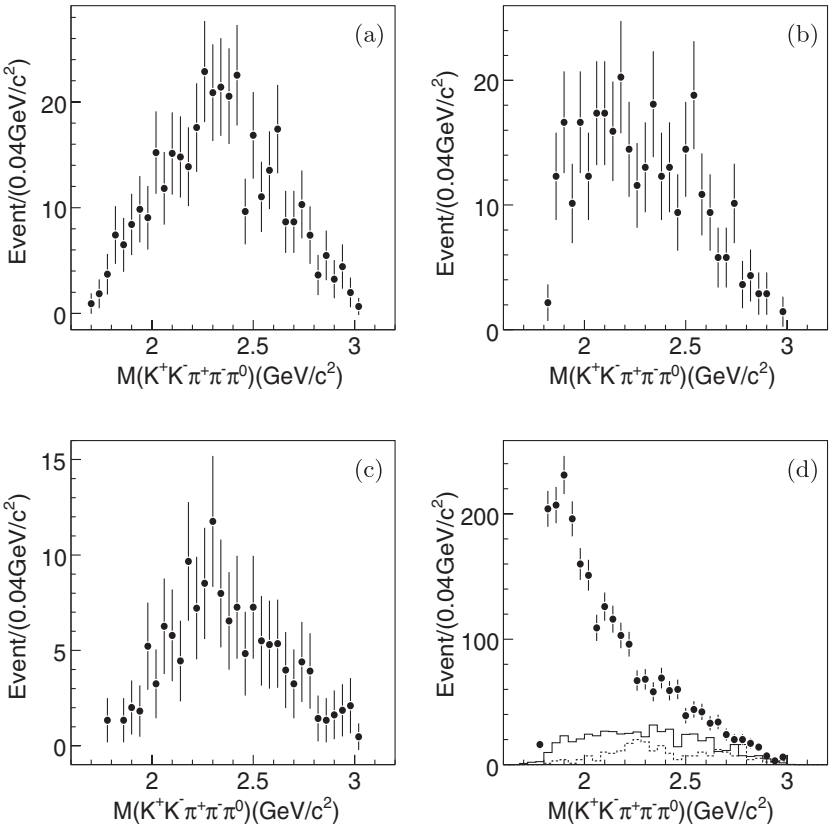

FIG. 3. The $K^+K^-\pi^+\pi^-\pi^0$ invariant-mass distribution for (a) the events in the ω sideband region [boxes A in Fig. 1(a)]; (b) the events in the ϕ sideband region [box B in Fig. 1(a)]; (c) the events in the corner region [boxes C in Fig. 1(a)]; and (d) the events in the $\omega\phi$ signal region; the solid histogram is the background distribution estimated from the sideband events, the dashed histogram is that obtained from inclusive J/ψ decay MC samples.

The relative magnitudes and phases of the states are determined by an unbinned maximum likelihood fit of the measured cross section $d\sigma/d\Phi$. The basis of likelihood fitting is the calculation of the probability that a hypothesized probability distribution function can produce the data set under consideration. The probability to observe the ith event characterized by the measurement ξ_i is the differential cross section normalized to unity

$$P(\xi_i) = \frac{\omega(\xi_i)\epsilon(\xi_i)}{\int d\xi \omega(\xi)\epsilon(\xi)}, \tag{3}$$

where ξ_i is the measured four-momentum of γ, K^+, K^-, π^+, π^-, and π^0 for a given ith event, $\omega(\xi_i) \equiv (\frac{d\sigma}{d\Phi})_i$ and $\epsilon(\xi_i)$ is the detection efficiency. The joint probability density for observing the N events in the data sample is

$$\mathcal{L} = \prod_{i=1}^{N} P(\xi_i) = \prod_{i=1}^{N} \frac{\omega(\xi_i)\epsilon(\xi_i)}{\int d\xi \omega(\xi)\epsilon(\xi)}. \tag{4}$$

FUMILI [21] is used to optimize the fit parameters in order to achieve the maximum likelihood value. Technically, rather than maximizing $\mathcal{L}$, $\mathcal{S} = -\ln\mathcal{L}$ is minimized, i.e.,

$$\mathcal{S} = -\ln\mathcal{L} = -\sum_{i=1}^{N} \ln\left(\frac{\omega(\xi_i)}{\int d\xi \omega(\xi)\epsilon(\xi)}\right) - \sum_{i=1}^{N} \ln\epsilon(\xi_i). \tag{5}$$

In practice, the normalized integral $\int d\xi_i \omega(\xi_i)\epsilon(\xi_i)$ is evaluated using the $J/\psi \to \gamma\omega\phi$ phase space MC sample. For a given data set, the second term is a constant and has no impact on the relative changes of the $\mathcal{S}$ value. The details of the PWA fit process are described in Ref. [22]. In the minimization procedure, a change in log likelihood of 0.5 represents a one standard deviation effect for the one-parameter case and is used to evaluate statistical errors.

Conservation of J^{PC}, in the $J/\psi \to \gamma X$, $X \to \omega\phi$ process in the case of a pseudoscalar intermediate resonance X, allows only $\mathcal{P}$ wave contributions in both the radiative decay $J/\psi \to \gamma X$ and the hadronic decay $X \to \omega\phi$. For the production of a 0^{++}, 1^{++} or 2^{++} resonance, both $\mathcal{S}$ and $\mathcal{D}$ waves are possible for both the radiative and hadronic decays, but only the $\mathcal{S}$ wave contribution is considered in the fit, since the $\mathcal{D}$ wave can be expected to be highly suppressed near the mass threshold. Intermediate X structures with $J^{PC} = 2^{-+}$ or higher spin are not considered in the analysis. To investigate the J^{PC} of the $X(1810)$, we tried

different J^{PC} assignments in the fit, and the assignment with the best log likelihood value is identified as the J^{PC} of the $X(1810)$. Some known mesons, e.g., $f_2(1950)$ or $f_0(2020)$, with a mass above the $\omega\phi$ invariant-mass threshold, are expected to decay to $\omega\phi$ final states and will be included in the PWA fit. To consider the contribution from coherent nonresonant component, an amplitude modeled by the same sequential process with a very broad (i.e., $M = 2500$ MeV and $\Gamma = 5000$ MeV) and a given J^{PC} intermediate state X will be included in the PWA fit, and the corresponding J^{PC} is determined by the optimization of the likelihood fit. The background event contribution to the log likelihood value is estimated from the weighted events in the sideband region and subtracted in the fit.

In the PWA fit, different J^{PC} combinations of the $X(1810)$ structure and the coherent nonresonant component, as well as different combinations of additional mesons listed in the PDG tables, are tried. The mass and width of the $X(1810)$ are determined by a scan of the maximum log likelihood value, while the mass and width of the additional mesons are fixed with their PDG values. The statistical significance of the state is determined by the changes of the maximum log likelihood value and of the number of degrees of freedom (Δndf) in the PWA fits with or without the state included. Only states with statistical significance larger than 5σ are included in the best solution.

We started the PWA fit with all possible intermediate states listed in the PDG tables. The state with the smallest statistical significance is removed from the fit one by one until all the states in the fit with statistical significance are larger than 5σ. Finally, together with the contributions of the $X(1810)$ and the coherent nonresonant component, additional 0^{++}, 2^{++}, and 0^{-+} components are found ($>5\sigma$) in the best solution of the PWA fit. In the following, the masses and widths of the 0^{++}, 2^{++}, and 0^{-+} components are assigned to be those of $f_0(2020)$, $f_2(1950)$, and $\eta(2225)$, respectively, since the fit with these has the best log likelihood value. Various PWA fits with different 0^{++}, 2^{++}, and 0^{-+} components were also performed. The results for the $X(1810)$ are robust, while the fit is not very sensitive to the masses and widths of the 0^{++}, 2^{++}, and 0^{-+} components. The log likelihood value changes are rather small when the $f_0(2020)$, $f_2(1950)$, and $\eta(2225)$ are replaced by other resonances with the same J^{PC} and similar masses. The details are shown below. The $J^{PC} = 0^{++}$ assignment for the $X(1810)$ has by far the highest log likelihood value among the different J^{PC} hypotheses. The minus log likelihood value ($\mathcal{S}$) for a $J^{PC} = 0^{++}$ assignment to the $X(1810)$ is 227 below that of the second lowest value (obtained for a $J^{PC} = 2^{++}$ assignment), and is 783 below that for a fit with the $X(1810)$ omitted. The latter corresponds to a statistical significance of more than 30σ. Different J^{PC} assignments for the coherent nonresonant component are tested in the PWA fit and $J^{PC} = 0^{-+}$ is favored. The assigned values for the J^{PC}, mass, width and number of events for the five components for the best fit solution are summarized in Table I. The mass and width of the $X(1810)$ are obtained to be $M = (1795 \pm 7)$ MeV/c^2 and $\Gamma = (95 \pm 10)$ MeV/c^2, respectively, where the errors are statistical only. The contributions of each component of the best solution of the PWA fit are shown in Fig. 4(a). The changes of the log likelihood value $\Delta\mathcal{S}$ and of the number of degrees of freedom Δndf that occur when a state is dropped from the PWA fit, as well as the corresponding statistical significance, are also listed in Table I. The statistical significance of the $f_2(1950)$, $f_0(2020)$, and $\eta(2225)$ contributions are 20.4σ, 13.9σ, and 6.4σ, respectively. The reconstruction and final-selection efficiency of the $X(1810)$ is determined from a weighted phase space MC sample of $J/\psi \to \gamma\omega\phi$, where the weight is the differential cross section for the measured events calculated with the magnitudes and phases of the partial amplitudes from the best solution of the PWA fit. The efficiency is determined to be 6.8% and the corresponding branching fraction is $\mathcal{B}(J/\psi \to \gamma X(1810)) \times \mathcal{B}(X(1810) \to \omega\phi) = (2.00 \pm 0.08) \times 10^{-4}$, where the error is statistical only.

The invariant-mass spectra $M(K^+K^-\pi^+\pi^-\pi^0)$, $M(\gamma\pi^+\pi^-\pi^0)$, $M(\gamma K^+K^-)$ and the $\cos\theta_\gamma$, $\cos\theta_\omega$, $\cos\theta_\phi$, $\cos\theta_K$, ϕ_ϕ, and χ angular distributions of the data and the PWA fit projections with the best solution as well as the different components are shown in Fig. 4. Here the angles θ_γ, θ_ω, θ_ϕ, and θ_K are the polar angles of the radiative photon in the J/ψ rest frame (respect to beam direction), the normal to the ω decay plane in the ω system, ϕ meson momentum direction in the $\omega\phi$ rest system, and the kaon from ϕ decay in the ϕ rest system, respectively; ϕ_ϕ is the azimuthal angle of the ϕ meson in the $\omega\phi$ system and χ is the angle between azimuthal angles of the normal to the ω decay plane and the momentum of a kaon from ϕ decay in the $\omega\phi$ system. The PWA fit projection is the sum of the number of events from the

TABLE I. Results from the best PWA fit solution.

Resonance	J^{PC}	M(MeV/c^2)	Γ(MeV/c^2)	Events	$\Delta\mathcal{S}$	Δndf	Significance
$X(1810)$	0^{++}	1795 ± 7	95 ± 10	1319 ± 52	783	4	$>30\sigma$
$f_2(1950)$	2^{++}	1944	472	665 ± 40	211	2	20.4σ
$f_0(2020)$	0^{++}	1992	442	715 ± 45	100	2	13.9σ
$\eta(2225)$	0^{-+}	2226	185	70 ± 30	23	2	6.4σ
Coherent nonresonant component	0^{-+}	...	...	319 ± 24	45	2	9.1σ

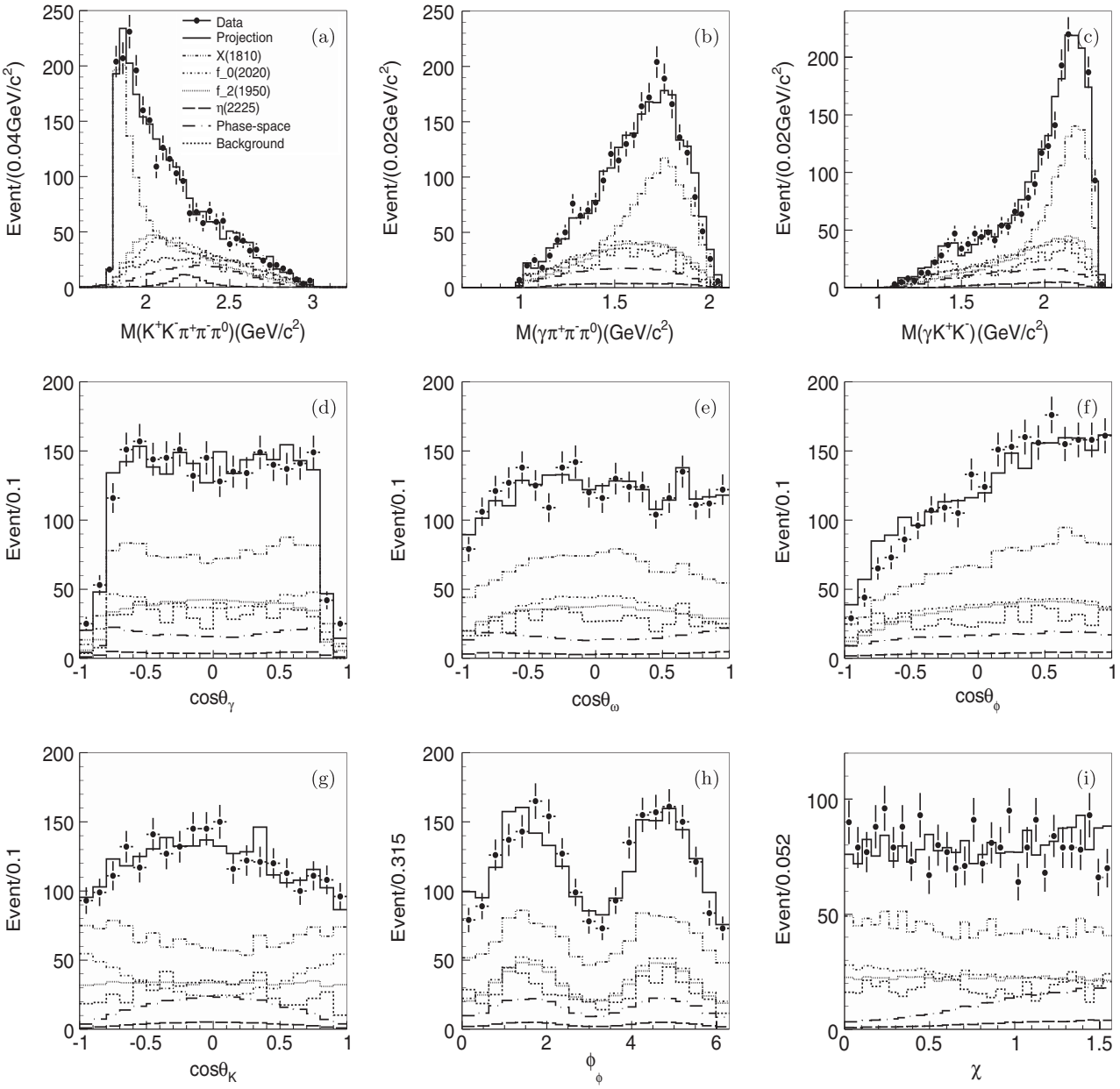

FIG. 4. Comparisons between data and PWA fit projections: (a) the $K^+K^-\pi^+\pi^-\pi^0$ invariant-mass distribution; (b) the $\gamma\pi^+\pi^-\pi^0$ invariant-mass distribution; (c) the γK^+K^- invariant-mass distribution; (d) the polar angle of the radiative photon (θ_γ) in the J/ψ system; (e) the polar angle of the normal to the ω decay plane in the ω system (θ_ω); (f) the polar angle of the ϕ in the $\omega\phi$ rest system (θ_ϕ); (g) the polar angle of the kaon in the ϕ rest system (θ_K); (h) the azimuthal angle of the ϕ in the $\omega\phi$ system; and (i) the distribution of χ which is the angle between azimuthal angles of the normal to the ω decay plane and the momentum of a kaon from ϕ decay in the $\omega\phi$ system. The dots with error bars are data, the solid histograms are the PWA fit projection, and the other histograms represent for the different signal components and background.

signal component in the best solution and the background estimated from the weighted events in the sideband region.

To determine the goodness of fit, a χ^2 is calculated by comparing the data and fit projection histograms, where χ^2 is defined as [22]

$$\chi^2 = \sum_{i=1}^{N} \frac{(n_i - \upsilon_i)^2}{\upsilon_i}, \tag{6}$$

and n_i and υ_i are the number of events for the data and the fit projections with best solution in the ith bin of each figure, respectively. The χ^2 and the number of degrees of freedom (ndf) for each mass and angular distribution are shown in Table II, where the number of bins is taken as the number of degrees of freedom. The values of χ^2/ndf range between 0.62 and 1.70, indicating reasonable agreement between data and the fit.

TABLE II. Goodness of fit check for the invariant-mass distributions and angular distributions shown in Fig. 4.

Variable	$M(K^+K^-\pi^+\pi^-\pi^0)$	$M(\gamma\pi^+\pi^-\pi^0)$	$M(\gamma K^+K^-)$	θ_γ	θ_ω	θ_ϕ	θ_K	ϕ_ϕ	χ
χ^2	44.4	36.4	42.4	24.2	12.4	28.2	18.2	26.4	51.0
ndf	40	35	40	20	20	20	20	20	30
χ^2/ndf	1.11	1.04	1.06	1.21	0.62	1.41	0.91	1.32	1.70

Additional fits with different assumptions have been carried out to check the influence on the parameters of the $X(1810)$. The masses and widths for the $f_2(1950)$, $f_0(2020)$, and $\eta(2225)$ are difficult to determine accurately from this analysis and the achieved accuracy cannot compete with the PDG accuracy because of the dominant $X(1810)$ component; instead, they are fixed to their PDG values in the fits. If we change the masses and widths of these three mesons by one standard deviation in the fitting, the log likelihood value changes by $\Delta\mathcal{S} < 3$ after refitting mass and width of the $X(1810)$; these values and the branching fraction remain consistent within the statistical errors. The maximum difference is taken as a systematic error. An alternative method to test the influence of the parameters of the three known mesons is to replace the mesons by states listed in the PDG tables with the same J^{PC} and similar mass. When the parameters of $f_2(1950)$ are replaced with those of the $f_2(1910)$, the log likelihood value increases by $\Delta\mathcal{S} = 6$ after refitting the mass and width of the $X(1810)$. When the parameters of $f_0(2020)$ are replaced with those of the $f_0(2100)$, the log likelihood value increases by $\Delta\mathcal{S} = 13$. If the $f_0(2020)$ is replaced with 0^{++} coherent nonresonant component, the log likelihood value increases by $\Delta\mathcal{S} = 9$. If the $f_2(1950)$ is replaced with $f_2(1910)$ and the $f_0(2020)$ is replaced with a 0^{++} coherent nonresonant component, the log likelihood value increases by $\Delta\mathcal{S} = 10$ after refitting. By comparing the log likelihood values, the combination of $X(1810)$, $f_2(1950)$, $f_0(2020)$, $\eta(2225)$, and $J^{PC} = 0^{-+}$ for the coherent nonresonant component is found to be the best solution, and the mass, width and branching fraction of $X(1810)$ changes are less than twice the statistical errors.

The states listed in the PDG tables with mass above the $\omega\phi$ threshold that are consistent with decaying into $\omega\phi$ under spin-parity constraints are the $f_2(1810)$, $f_2(1910)$, $f_2(2010)$, $f_0(2100)$, $f_2(2150)$, $f_0(2200)$, $f_2(2300)$, and $f_2(2340)$, etc. Relative to the best solution of the PWA fit, as these resonances are added in the fit, the log likelihood value improves by 7.0, 11.7, 8.1, 1.5, 3.2, 1.7, 2.5, and 0.9 after refitting the mass and width of the $X(1810)$, and the statistical significance of these additional resonances are all less than 5σ, while the mass, width and branching fraction of $X(1810)$ are consistent with those from the best solution within statistical errors. The maximum difference between the best fit result and the result with extra states included is taken as a systematic error. In the best fit solution, coherent nonresonant component is included and approximated as a broad $J^{PC} = 0^{-+}$ resonance. An additional coherent nonresonant component amplitude with different J^{PC} was added to test whether the data contain different J^{PC} coherent nonresonant component. When the fit is redone including additional coherent nonresonant component with $J^{PC} = 0^{++}$, 1^{++}, 2^{++}, the log likelihood value improves by 0.1, 3.8, and 3.7, respectively. No evidence of coherent nonresonant component with different J^{PC} values is found, while the $X(1810)$ mass, width and branching fraction are consistent with best solution within statistical errors. The maximum differences are taken as systematic errors. The BESIII collaboration has observed two new pseudoscalar resonances, $X(1835)$ in the $J/\psi \to \gamma\eta'\pi^+\pi^-$ decay process [23] and the $X(p\bar{p})$ in the $J/\psi \to \gamma p\bar{p}$ decay process [24]. It is interesting to know whether either of these has a $\omega\phi$ decay mode. Based on the best solution of the PWA fit, new pseudoscalar states with $M = 1836.5$ MeV/c^2, $\Gamma = 190.1$ MeV/c^2 and $M = 1832$ MeV/c^2, $\Gamma = 76$ MeV/c^2 are added in the fit, respectively. The log likelihood value improves by 2.2 and 3.5, and corresponding statistical significance is 1.1σ and 1.6σ, respectively.

Based on the best solution, a more general test is carried out to investigate the possible contribution from additional resonances not listed by the PDG. Additional resonances with specified J^{PC} and width are included (one at a time) in the fit, with a mass that ranges from low to high values. The scans are repeated with different widths and J^{PC} values. We find that any additional state contribution has a statistical significance that is less than 5σ, and the mass, width and branching fraction of the $X(1810)$ found in this way are consistent with the best solution. This method is used to test whether a new resonance/state can be included in the data and no evidence for a new extra resonance is observed. The differences in the $X(1810)$ parameters due to the possible presence of an additional resonance are not considered in the systematic error determination.

V. SYSTEMATIC UNCERTAINTY STUDY

For studies of the systematic uncertainties on the PWA-determined mass, width and branching fraction values for the $X(1810)$, in addition to those discussed above, the effect of different background determination has also been studied. To estimate the systematic uncertainty associated with the background determination, the sideband regions (requirements III and IV) are shifted away from the signal region by 40 MeV/c^2 and 15 MeV/c^2 in the $\pi^+\pi^-\pi^0$ and K^+K^- invariant masses, respectively, the sideband normalization factors are re-evaluated, and the PWA fit is

redone using the same procedure. The differences from the best solution are taken as systematic errors.

For the systematic errors on the branching fraction measurement, there are additional uncertainties from tracking efficiency, particle identification, photon detection, kinematic fit, as well as the branching fraction of the intermediate states and the total number of J/ψ events.

The systematic uncertainty associated with the tracking efficiency has been studied with $J/\psi \to \pi^+\pi^- p\bar{p}$ and $J/\psi \to K^0_S K\pi$, $K^0_S \to \pi^+\pi^-$ control samples [25]. The difference between data and MC is 2% per charged pion and kaon track. Here, 8% is taken as the systematic error for the detection efficiency of charged tracks.

The uncertainty due to the kaon particle identification is determined from studies of a $J/\psi \to K^* K$ control sample [25]. The difference in the particle identification efficiency between data and MC is 1% per kaon. Here, 2% is taken as systematic error for the identification of two kaons.

The uncertainty due to photon detection efficiency is 1% per photon, which is determined from a $J/\psi \to \rho\pi$ control sample [25]. Here, 3% is taken as systematic error for the efficiency of the three photon detection.

To estimate the uncertainty associated with kinematic fit, selected samples of $\psi(2S) \to \pi^+\pi^- J/\psi$, $J/\psi \to K^+K^-\pi^0$ and $\psi(2S) \to \pi^+\pi^- J/\psi$, $J/\psi \to K^+K^-\pi^0\pi^0$ events are used to study efficiency differences between data and MC. The efficiency associated with kinematical fit for these control samples are defined as the ratio between the number of events with and without the 4C-fit cut in each of the MC and experimental data samples. The efficiency differences between data and MC are 4.2% and 7.0% for the two samples, respectively. Compared to the final states of the studied channel, the two control samples have exactly the same charged tracks but one more or one less photon. Conservatively, 7.0% is taken as the systematic error associated with the kinematic fit.

For the branching fractions of $\phi \to K^+K^-$, $\omega \to \pi^+\pi^-\pi^0$, and $\pi^0 \to \gamma\gamma$ decays, the uncertainty on these branching fractions listed in the PDG tables [18] are taken as a systematic uncertainty for our measurement. The total number of J/ψ events is $(225.3 \pm 2.8) \times 10^6$, determined from inclusive J/ψ hadron decays [10], with an uncertainty of 1.2%.

A summary of all the uncertainties is shown in Table III. The total systematic uncertainty is obtained by summing up all uncertainty contributions in quadrature. The systematic uncertainties on the mass and width of the $X(1810)$ are $^{+13}_{-5}$ MeV/c^2 and $^{+21}_{-34}$ MeV/c^2, respectively, and the relative systematic error on the product branching fraction is $^{+22}_{-50}$%.

In the best PWA fit, the threshold enhancement $X(1810)$ is parametrized by a Breit-Wigner formula with a constant width. Since the enhancement structure is near the $\omega\phi$ threshold, other decay modes of $X(1810)$ are expected. To account for this, the Flatté formula [26] is used to parametrize the structure $X(1810)$. We assume the $X(1810)$ mainly decays to $\omega\phi$ and K^+K^- final states, and $g_{\omega\phi}$ and g_{KK} are the coupling constants to the two modes, respectively. We test two cases, one with $g_{\omega\phi} = 1$, $g_{KK} = 0$ and the other with $g_{\omega\phi} = 0.5$, $g_{KK} = 0.5$, the mass and width of the $X(1810)$ shift by ± 19 MeV/c^2 and ± 75 MeV/c^2, respectively, and while the relative change in the product branching ratio is ± 65.1%. These are considered as a second systematic error due to uncertainty of the model dependence.

VI. SUMMARY AND DISCUSSION

We use $(225.3 \pm 2.8) \times 106$ J/ψ events accumulated with the BESIII detector to study the doubly OZI-suppressed decays of $J/\psi \to \gamma\omega\phi$, $\omega \to \pi^+\pi^-\pi^0$, $\phi \to K^+K^-$. A strong deviation from three-body phase space for $J/\psi \to \gamma\omega\phi$ near the $\omega\phi$ invariant-mass threshold is observed. Assuming the enhancement is due to the influence of a resonance, the $X(1810)$, a partial wave analysis with a tensor covariant amplitude determines that the spin-parity of the $X(1810)$ is 0^{++}, and the statistical

TABLE III. Summary of systematic errors of the mass, width and branching ratio (B.R.) (in percentage) of $X(1810)$.

Source	Mass (MeV/c^2)	Width (MeV/c^2)	B.R. (%)
Tracking efficiency	···	···	8.0
Particle identification	···	···	2.0
Photon detection	···	···	3.0
Kinematic fit	···	···	7.0
Intermediate branching ratio	···	···	1.3
J/ψ total number	···	···	1.2
Components in the best fit	+2.0 −5.1	+12.8 −6.7	+19.1 −26.1
Resonance parametrization	+12.2 −1.0	+17.3 −33.0	+1.6 −40.8
Background estimation	+3.0	−1.0	−1.4
Total	+12.8 −5.2	+21.4 −33.7	+22.3 −49.8

significance of the $X(1810)$ is more than 30σ. The mass and width of the $X(1810)$ are determined to be $M = 1795 \pm 7(\text{stat}) + 13 - 5(\text{syst}) \pm 19(\text{mod})\ \text{MeV}/c^2$ and $\Gamma = 95 \pm 10(\text{stat}) + 21 - 34(\text{syst}) \pm 75(\text{mod})\ \text{MeV}/c^2$ and the product branching fraction is measured to be $\mathcal{B}(J/\psi \to \gamma X(1810)) \times \mathcal{B}(X(1810) \to \omega\phi) = (2.00 \pm 0.08(\text{stat}) + 0.45 - 1.00(\text{syst}) \pm 1.30(\text{mod})) \times 10^{-4}$, where the first error indicates the statistical error and the second is the systematical error. These results are consistent within errors with those from the BESII experiment [1].

The decay $J/\psi \to \gamma\omega\phi$ is a doubly OZI-suppressed process that is expected to be suppressed relative to $J/\psi \to \gamma\omega\omega$ or $J/\psi \to \gamma\phi\phi$ by at least one order of magnitude [2]. The anomalous enhancement observed at the $\omega\phi$ invariant-mass threshold and the large measured branching fractions ($\sim 1/2$ of $\mathcal{B}(J/\psi \to \gamma\phi\phi)$ [18]) are surprising and interesting. The enhancement is not compatible with being due either to the $X(1835)$ or the $X(p\bar{p})$, due to the different mass and spin-parity. The interpretation of the enhancement as being due to effects of $\omega\phi$ final state interactions is not excluded in this analysis. Searches for this structure in different decays modes, e.g., K^*K^*, $\omega\omega$, etc., and in other production processes, e.g., $J/\psi \to \phi\omega\phi$, $J/\psi \to \omega\omega\phi$, etc., are essential to explore the nature of the enhancement, and gain more insight in the underlying dynamics. The search for other possible states decaying to $\omega\phi$ would also be of interest. Contributions from 0^{++}, 0^{-+}, 2^{++} partial waves are found to be necessary in the PWA fit and simply assigned to the $f_0(2020)$, $\eta(2225)$, and $f_2(1950)$, respectively, in this analysis, since the dominant contribution in the decay is the process with intermediate state $X(1810)$, and the PWA fit is not sensitive to those masses and widths.

ACKNOWLEDGMENTS

The BESIII collaboration thanks the staff of BEPCII and the computing center for their hard efforts. This work is supported in part by the Ministry of Science and Technology of China under Contract No. 2009CB825200; National Natural Science Foundation of China (NSFC) under Contracts No. 10625524, No. 10821063, No. 10825524, No. 10835001, No. 10875113, No. 10935007, No. 11125525, No. 10979038, No. 11005109, No. 11079030, and No. 11275189; Joint Funds of the National Natural Science Foundation of China under Contracts No. 11079008, No. 11179007; the Chinese Academy of Sciences (CAS) Large-Scale Scientific Facility Program; CAS under Contracts No. KJCX2-YW-N29, No. KJCX2-YW-N45; 100 Talents Program of CAS; Research Fund for the Doctoral Program of Higher Education of China under Contract No. 20093402120022; Istituto Nazionale di Fisica Nucleare, Italy; Ministry of Development of Turkey under Contract No. DPT2006K-120470; U.S. Department of Energy under Contracts No. DE-FG02-04ER41291, No. DE-FG02-91ER40682, and No. DE-FG02-94ER40823; U.S. National Science Foundation, University of Groningen (RuG) and the Helmholtzzentrum fuer Schwerionenforschung GmbH (GSI), Darmstadt; and WCU Program of National Research Foundation of Korea under Contract No. R32-2008-000-10155-0.

[1] M. Ablikim *et al.* (BES Collaboration), Phys. Rev. Lett. **96**, 162002 (2006).
[2] L. Köpke and N. Wermes, Phys. Rep. **174**, 67 (1987).
[3] B. A. Li, Phys. Rev. D **74**, 054017 (2006).
[4] K. T. Chao, arXiv:hep-ph/0602190.
[5] P. Bicudo, S. R. Cotanch, F. J. Llanes-Estrada, and D. G. Robertson, Eur. Phys. J. C **52**, 363 (2007).
[6] Q. Zhao B.-S. Zou, Phys. Rev. D **74**, 114025 (2006).
[7] A. M. Torres *et al.*, arXiv:1210.6392v1.
[8] D. V. Bugg, J. Phys. G **35**, 075005 (2008).
[9] C. Liu *et al.* (Belle Collaboration), Phys. Rev. D **79**, 071102(R) (2009).
[10] M. Ablikim *et al.* (BESIII Collaboration), Chinese Phys. C **36**, 915 (2012).
[11] M. Ablikim *et al.* (BESIII Collaboration), Nucl. Instrum. Methods Phys. Res., Sect. A **614**, 345 (2010).
[12] J. Z. Bai *et al.* (BES Collaboration), Nucl. Instrum. Methods Phys. Res., Sect. A **344**, 319 (1994); **458**, 627 (2001).
[13] S. Agostinelli *et al.* (GEANT4 Collaboration), Nucl. Instrum. Methods Phys. Res., Sect. A **506**, 250 (2003).
[14] Z. Y. Deng *et al.*, HEP & NP **30**, 371 (2006).
[15] S. Jadach, B. F. L. Ward, and Z. Was, Comput. Phys. Commun. **130**, 260 (2000).
[16] S. Jadach, B. F. L. Ward, and Z. Was, Phys. Rev. D **63**, 113009 (2001).
[17] R. G. Ping, Chinese Phys. C **32**, 599 (2008).
[18] J. Beringer *et al.* (Particle Data Group), Phys. Rev. D **86**, 010001 (2012).
[19] J. C. Chen, G. Huang, X. Qi, D. Zhang, and Y. Zhu, Phys. Rev. D **62**, 034003 (2000).
[20] S. Dulat and B. S. Zou, Eur. Phys. J. A **26**, 125 (2005).
[21] I. Silin, CERN Program library Report No. D510, 1971.
[22] M. Ablikim *et al.* (BES Collaboration), Phys. Rev. D **72**, 092002 (2005).
[23] M. Ablikim *et al.* (BES Collaboration), Phys. Rev. Lett. **106**, 072002 (2011).
[24] M. Ablikim *et al.* (BES Collaboration), Phys. Rev. Lett. **108**, 112003 (2012).
[25] M. Ablikim *et al.* (BES Collaboration), Phys. Rev. D **83**, 112005 (2011).
[26] S. M. Flatté, Phys. Lett. **63B**, 224 (1976).